

# Probing the Band Topology of Mercury Telluride through Weak Localization and Antilocalization

Viktor Krueckl and Klaus Richter

*Institut für Theoretische Physik, Universität Regensburg, D-93040 Regensburg, Germany*

We analyze the effect of weak localization (WL) and weak antilocalization (WAL) in the electronic transport through HgTe/CdTe quantum wells. We show that for increasing Fermi energy the magnetoconductance of a diffusive system with inverted band ordering features a transition from WL to WAL and back, if spin-orbit interactions from bulk and structure inversion asymmetry can be neglected. This, and an additional splitting in the magnetoconductance profile, is a signature of the Berry phase arising for inverted band ordering and not present in heterostructures with conventional ordering. In presence of spin-orbit interaction both band topologies exhibit WAL, which is distinctly energy dependent solely for quantum wells with inverted band ordering. This can be explained by an energy-dependent decomposition of the Hamiltonian into two blocks.

PACS numbers: 05.60.Gg, 73.23.-b, 85.35.Ds

## I. INTRODUCTION

The first theoretical proposal for a two-dimensional topological insulator was based on graphene with intrinsic spin-orbit interaction (SOI) [1, 2]. Although the spin-orbit coupling of graphene is too small to render an experimental evidence [3, 4], this initiated several other suggestions for two-dimensional materials and heterostructures showing topological insulator features [5–7]. Subsequently, the criteria for topological insulators were extended to three dimensions [8] and were experimentally verified in other suitable materials like BiSe [9] or Bi<sub>2</sub>Te<sub>3</sub> [10, 11]. In the meantime, the quantum spin Hall effect, a prominent transport feature of two-dimensional topological insulators, has been observed in HgTe/CdTe quantum wells [12, 13] as well as for InAs/GaSb heterostructures [14]. In both experiments the transmission through a mesoscopic Hall bar is quantized since the bulk of the system is insulating and the current is only carried by edge states, which are protected from backscattering due to time-reversal symmetry.

Whilst many theoretical investigations are focused on these edge states of two-dimensional topological insulators [15–19], signatures of the special band topology are also traceable in other observables even away from the bulk band gap. To this end we consider a well studied phenomenon in phase coherent transport through disordered quantum systems, namely weak localization (WL) [20] for systems without SOI and weak antilocalization (WAL) [21] in presence of SOI. The effect stems from the self interference of the charge carriers leading to a quantum correction to the classical transmission for time reversal symmetric systems. Breaking of this symmetry can be easily achieved by applying a perpendicular magnetic field. In a semiclassical picture, the effect is understood in terms of interference between waves traveling in opposite directions along backscattered paths and averaging over all such trajectory pairs. Besides the relative phase shift arising from the enclosed flux of an external

perpendicular magnetic field, intrinsic Berry phases affect the interference and thereby the WL behavior. As a consequence, the signatures of WL in transport through systems with strong Berry phases, as for example HgTe heterostructures, can differ significantly from those of conventional electron gases.

To our knowledge, there are only a few theoretical studies of WL in systems with inverted band ordering [22, 23]. Diagrammatic studies for the two-dimensional case with inverted band ordering show a transition between WL and WAL upon varying the chemical potential [23]. However, major SOI effects from bulk and inversion asymmetry are not included, which alter the WL signal, as we will show in this work. A recent experiment revealed WAL in diffusive transport [24] and detailed investigations attested an energy dependence of the WAL peak [25]. Since no theories for WL in heterostructures with inverted band ordering including SOI are at hand, only conventional theories for A<sub>3</sub>B<sub>5</sub> semiconductors [26, 27] have yet been applied to analyze these results.

In order to explore how WL effects are altered by the inverted band ordering of topological insulators, we perform numerical transport calculations. We confirm the transition between WL and WAL reported in Ref. [23], if SOI can be neglected. We explain the effect in terms of the Berry phase of the bands involved. Moreover, we additionally find a splitting of the WL magnetoconductance profiles due to the two spin species that can also be traced back to the Berry phase and is not accounted for in previous diagrammatic studies. Additionally, we show how the WL phenomenon is altered by SOI, and how bulk and structure inversion asymmetry lead to significantly different WAL features that can strongly depend on the band ordering.

This paper is structured as follows: In Section II we introduce the model used to describe multi-band quantum transport in diffusive HgTe heterostructures. In Section III we focus on effects of the Berry phase and the energy dependence of WL and WAL without SOI. In Sec-

tion IV we include SOI and show why a variation in WAL upon change in energy serves as an indicator for inverted band ordering. Finally, in Section V we conclude with a brief summary.

## II. MODEL

We describe the electronic properties of the underlying HgTe heterostructure by the Hamiltonian [5, 28]

$$H = \begin{pmatrix} C_k + M_k & Ak_+ & -iRk_- & -\Delta \\ Ak_- & C_k - M_k & \Delta & 0 \\ iRk_+ & \Delta & C_k + M_k & -Ak_- \\ -\Delta & 0 & -Ak_+ & C_k - M_k \end{pmatrix} \quad (1)$$

where  $k_{\pm} = k_x \pm ik_y$ ,  $\mathbf{k}^2 = k_x^2 + k_y^2$ ,  $C_k = D\mathbf{k}^2$  and  $M_k = M - B\mathbf{k}^2$ . The material parameters are chosen to be  $A = 354.5 \text{ meV nm}$ ,  $B = -686 \text{ meV nm}$ ,  $D = -512 \text{ meV nm}^2$  and  $M = \pm 10 \text{ meV}$ . Without SOI ( $R = \Delta = 0$ ) this Hamiltonian breaks up into two independent  $2 \times 2$  blocks, each consisting of an  $s$ -like electron and a  $p$ -like hole band. The topology of the band structure depends on the ordering of the electron and hole states, given by the gap  $M$  which is positive for conventional ordering ( $M > 0$ ) and negative for inverted ordering ( $M < 0$ ).

Additionally, in Section IV we take into account the SOI of strength  $\Delta$  and  $R$  due to bulk inversion asymmetry (BIA) as well as structure inversion asymmetry (SIA) [28]. While  $\Delta$  is fixed (we use  $\Delta = 1.6 \text{ meV}$  [29]), the strength of the SOI due to SIA depends on the quantum well structure, and can be tuned to very small values by growing symmetric wells.

We study the signatures of WL in magnetotransport through diffusive conductors in the presence of a perpendicular magnetic field  $B$ . We consider coherent two-terminal transport through disordered strip geometries with a Gaussian correlated disorder,

$$U(\mathbf{r}) = \sum_i U_i \exp\left(-\frac{(\mathbf{r} - \mathbf{R}_i)^2}{2\sigma^2}\right), \quad (2)$$

with a correlation length  $\sigma$ . Here, a box distribution,  $-U_0 \leq U_i \leq U_0$ , is chosen for the strength  $U_i$  of the impurity  $i$  located at  $\mathbf{R}_i$ . In order to eliminate the influence of the edge states we employ periodic boundary conditions in the scattering region, linking the upper and lower edges along transport direction as sketched in Fig 1 (a). We discretize the Hamiltonian (1) on a square grid with a lattice spacing of 5 nm. The conductance

$$G = \frac{e^2}{h} T = \frac{e^2}{h} \sum_{n,m} \sum_{\sigma,\sigma'} |t_{m,\sigma';n,\sigma}|^2 \quad (3)$$

is calculated in linear response within the Landauer formalism [30], whereby the transmission amplitudes  $t_{m,\sigma';n,\sigma}$  are given by the Fisher-Lee relations [31]. The

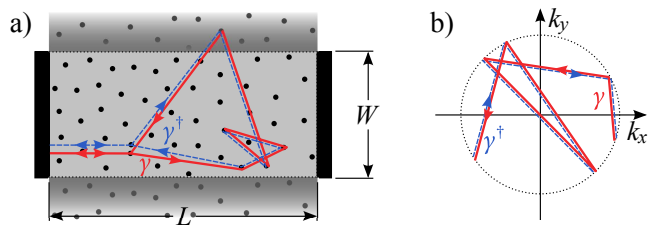


FIG. 1: a) Sketch of the scattering region with periodic boundary conditions in vertical direction between two non-periodic leads. A typical backscattered path and its time reversed counter path are shown, contributing to WL and WAL. b) Corresponding momentum-space trajectory for the two paths of (a).

indices  $m$  and  $n$  stand for the different modes in the leads, which are additionally classified through the index  $\sigma \in \{U, L\}$  denoting the upper left (U) and the lower right (L) block of the Hamiltonian (1) if no SOI is present ( $\Delta = R = 0$ ).

## III. BERRY PHASE EFFECTS IN QUANTUM TRANSPORT WITHOUT SPIN-ORBIT INTERACTION

In the following, we assume a negligibly small BIA and SIA spin-orbit interaction leading to a Hamiltonian (1) with two uncoupled blocks. We will show that the Berry phase of each of those blocks leads to an energy dependence of the WL signal different for the two band orderings. Without losing generality we focus on the upper subblock

$$H_U = \begin{pmatrix} M - (B + D)\mathbf{k}^2 & A(k_x + ik_y) \\ A(k_x - ik_y) & -M + (B - D)\mathbf{k}^2 \end{pmatrix}, \quad (4)$$

since the results for the lower subblock can be obtained by applying the time reversal operator. This Hamiltonian can be easily diagonalized, leading to the energy dispersion for the electron and hole branch,

$$E_{e/h}(\mathbf{k}) = -D\mathbf{k}^2 \pm F(\mathbf{k}), \quad (5)$$

with

$$F(\mathbf{k}) = \sqrt{A^2\mathbf{k}^2 + (B\mathbf{k}^2 - M)^2}. \quad (6)$$

The corresponding eigenstates are given by

$$\psi_{e/h}(\mathbf{k}) \propto \begin{pmatrix} M - B\mathbf{k}^2 \pm F(\mathbf{k}) \\ A(k_x - ik_y) \end{pmatrix}. \quad (7)$$

For vanishing SOI, the WL properties are governed by the phases accumulated by one of these spinors. In a semiclassical description quantum corrections to the conductance stem from the interference of waves traveling along different impurity-scattered paths. Upon disorder average the contributions from pairs of uncorrelated

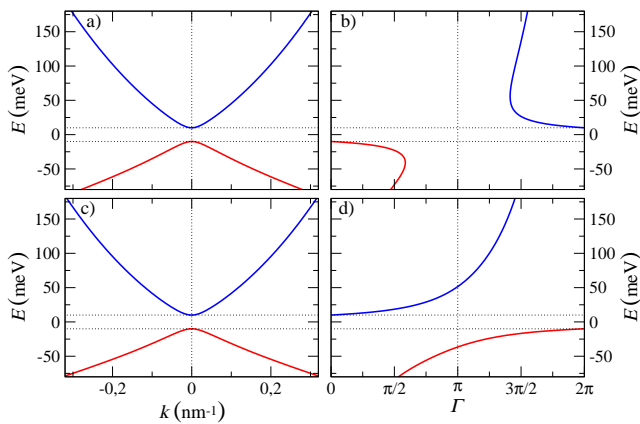


FIG. 2: Bulk band structure (a),(c) and corresponding Berry phase Eq. (9). (b),(d) of the Hamiltonian (1). Top panels show the result for conventional band ordering ( $M = 10$  meV), bottom panels the result for inverted band ordering ( $M = -10$  meV).

paths vanish. The remaining contributions leading to WL mainly originate from pairs of a path  $\gamma$  with its time inverted path  $\gamma^\dagger$  where the dynamical phases cancel out, as depicted in Fig. 1 (a). As a result, the WL signal is governed by additional phases, like the phase due to the flux of an external magnetic field or a Berry phase. The latter is associated with the Berry curvature given by [32, 33]

$$\mathcal{A}_\sigma(\mathbf{k}) = -i\langle\psi_\sigma(\mathbf{k})|\nabla_{\mathbf{k}}\psi_\sigma(\mathbf{k})\rangle, \quad (8)$$

in terms of the bulk eigenstates  $\psi_\sigma(\mathbf{k})$ . The corresponding phase is obtained by integrating the vector potential  $\mathcal{A}_\sigma$  along a backscattered path corresponding to a closed loop in momentum space with a fixed momentum  $k = |\mathbf{k}|$ , as sketched in Fig. 1 (b):

$$\Gamma_\sigma = \oint_{k=\text{const}} \mathcal{A}_\sigma(\mathbf{k}) \cdot d\mathbf{k} = 2\pi \mathcal{A}_\sigma(\mathbf{k}) \cdot (-k_y, k_x). \quad (9)$$

Because of the circular symmetry of  $\mathcal{A}_\sigma(\mathbf{k})$  the phase  $\Gamma_\sigma$  can be evaluated by the scalar product  $\mathcal{A}_\sigma(\mathbf{k}) \cdot (-k_y, k_x)$  at a single point in momentum space. This geometric phase  $\Gamma_\sigma$  enters the semiclassical Greens function. As depicted in Fig. 1 (b), a backscattered path and its time-inverted partner accumulate opposite reflection angles in momentum space. In view of Eq. (9), this opposite angle leads to opposite Berry phases and thereby to a dephasing in the two-path interference. This results in a reduction of WL [34], right up to a complete reversal of the WL correction to full WAL [35, 36]. For the Hamiltonian (1) the geometric phase  $\Gamma_\sigma$  has remarkable properties depending on the two different band topologies. In the case of HgTe the strength of the geometric phase of the electron and the hole branch are given by

$$\Gamma_{e/h} = \pi \left( 1 \pm \frac{M - Bk^2}{F(\mathbf{k})} \right). \quad (10)$$

Although the band structure of the conventional ( $M > 0$ ) and inverted ( $M < 0$ ) ordering is very similar [compare Fig. 2 (a),(c)], the Berry phases of the different systems are not. For the inverted band ordering, the Berry phase spans the whole range of possible phases from 0 to  $2\pi$ , as shown in Fig. 2 (d). As a consequence, a particular energy exists where the accumulated phase  $\Gamma_\sigma = \pi$ , as in a “neutrino billiard” [37]. However, if the bands are ordered conventionally, this is not the case. Although the phase differs significantly from 0 or  $2\pi$ , the region around  $\pi$  is excluded as shown in Fig. 2 (b). As a consequence, we expect distinctly different WL behavior for both systems if the whole energy range is considered.

In the following, we study the WL correction in transport through a disordered HgTe heterostructure numerically by calculating the average change of the quantum transmission

$$\delta T(B) = \langle T(B) - T(0) \rangle \quad (11)$$

in presence of a perpendicular magnetic field  $B$ . We tune the Berry phase by changing the Fermi energy of the system. The averages are taken over a set of 1000 different impurity potentials (2) distributing 20000 impurities (equals a coverage of 10% of the grid points) within a scattering region of  $1000 \text{ nm} \times 5000 \text{ nm}$  with a correlation length  $\sigma = 15 \text{ nm}$ . The disorder strength  $U_0$  is tuned to get a constant mean free path of  $1200 \text{ nm}$  for all energies, leading to comparable shapes of the localization correction for a large range of Fermi energies.

The results are summarized in Fig. 3. For energies close to the band gap, the Berry phase is very small in both cases. As a result, the average transmission is similar to that of an electron gas, leading to WL, visible as a negative correction to the magnetotransmission and shown as black line in Fig. 3 (a) for the case of inverted band ordering. By increasing the Fermi energy also the Berry phase raises, leading to a reduced WL correction. For values of  $\Gamma_\sigma = \pi/2$ , the minimum in the average transmission at  $B = 0$  is expected to vanish, which is also reflected in the numerical data presented as green line in Fig. 3 (a). If the energy is tuned to

$$E_e^{(\pi)} = -\frac{DM}{B} + \sqrt{\frac{A^2M}{B}}, \quad (12)$$

such that the momentum  $\mathbf{k}$  fulfills  $Bk^2 = M$ , the regime with a Berry phase close to  $\pi$  is entered. In this configuration, the system is expected to feature WAL, since a path and the time inverted counter path accumulate a phase difference of  $\pi$  and therefore interfere destructively, leading to an enhanced transmission at  $B = 0$ . This is indeed visible in the numerical results (Fig. 3 (a) as blue line) showing a pronounced WAL peak.

The physics changes, if a heterostructure with conventional ordering of the quantum well states is considered. In Fig. 3 (b) we show the average magnetoconductance for the same configuration as in Fig. 3 (a), however, we assume a positive bandgap of  $M = 10 \text{ meV}$ . For Fermi

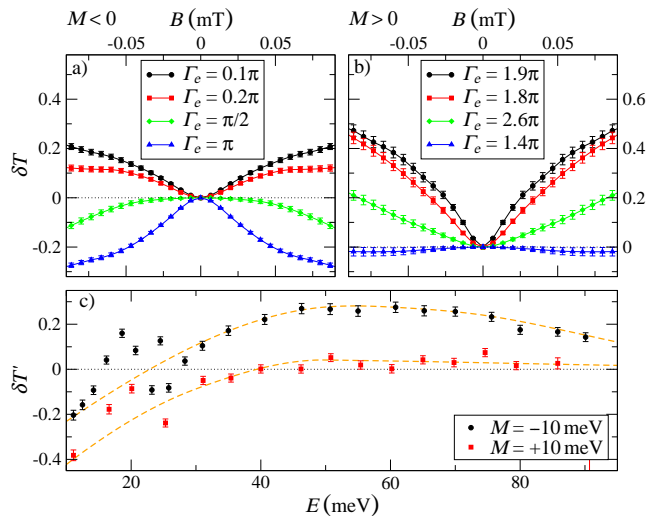


FIG. 3: Weak localization correction in a disordered HgTe nanoribbon ( $L = 5000$  nm,  $W = 1000$  nm). Upper panels: Magnetic field dependence for (a) inverted band ordering and (b) conventional ordering. Different Fermi energies ( $E_F = \{11.1$  meV,  $12.5$  meV,  $18.5$  meV,  $52$  meV $\}$  from top to bottom) lead to a Berry phase as given in panel (a) and (b). Impurity potential strength  $U_0$  is varied to fix a mean free path of  $1200$  nm. c) Energy dependence of the WL correction  $\delta T'$ , Eq. (13), for inverted and conventional ordering extracted for a magnetic field  $B = 0.1$  mT. Dashed curves are guides to the eye.

energies close to the bandgap, the Berry phase is small, as in the case with inverted band ordering, leading to a conventional WL feature. Unexpectedly, the strength of the WL correction of the conventional regime is almost twice as strong as the result for the inverted regime [compare black lines in Figs. 3 (a,b)]. With increasing Fermi energy, the strength of the Berry phase increases, but does not reach  $\pi$ . Instead, the maximal phase at  $Bk^2 = M$  is rather close to  $\pi/2$ , leading to a strong reduction of any localization correction [see blue line of Fig. 3 (b)].

For a more closer analysis of the energy dependence we extract the strength of the WL correction,

$$\delta T' = \langle T(B = 0) - T(B = 0.1 \text{ mT}) \rangle, \quad (13)$$

for various Fermi energies. The results are summarized in Fig. 3 (c). For conventional ordering, we get a transition from WL close to the band gap to almost no localization for higher energies. For inverted band ordering one finds a clear-cut transition, from WL to WAL and back to WL. Note that for very low energies only few channels contribute to transport. As a consequence the strength of the WL correction is reduced due to the finite number of open channels [38], and non-universal features may appear. These apparently erratic values vanish when the width of the scattering region is increased.

Additional to the expected crossover from WL to WAL, the Berry phase leads furthermore to opposite shifts in  $B$  of the magnetotransmission profiles associated

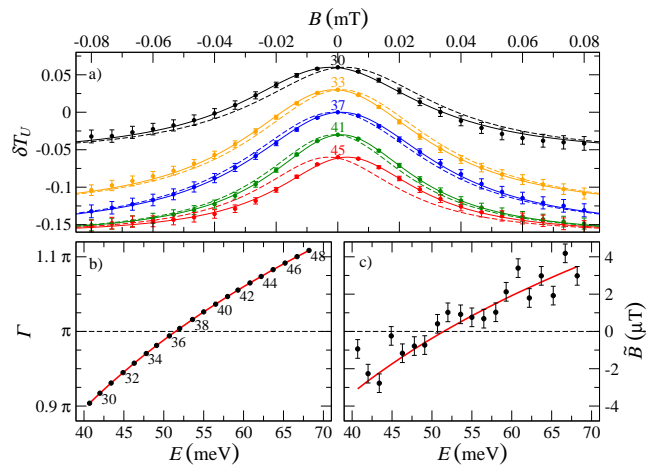


FIG. 4:  $B$ -field shift of the WAL maximum due to correlations between enclosed area and angle of the contributing trajectories. a) Magnetic field dependence of transmission quantum correction of a diffusive periodic nanoribbon ( $W = 1000$  nm,  $L = 5000$  nm) for different number of open channels (30 to 45) close to the Fermi energy  $E_F = 52$  meV (displayed with vertical offset). Symbols with error bars: Results  $\delta T_U$  for upper block, see Eq. (11); solid lines: fit to numerical data; dashed lines: corresponding curve for  $\delta T_L$  of lower block. b) Energy dependence of Berry phase around  $52$  meV (see Fig. 2 (a)). c) Energy dependence of shift  $\tilde{B}$  of the magnetotransmission maximum extracted from (a).

with the upper and lower blocks of the Hamiltonian (1). A pair of backscattered paths, contributing to WL and WAL, can be characterized in terms of the enclosed area  $A$  and the accumulated angle  $\alpha$ , acquired during the series of random scattering processes at impurities along the diffusive path. Usually, only the enclosed areas  $A$  are relevant, and their typical value  $A_0$  sets the magnetic field scale in the magnetoconductance profile; *i.e.* its width is of order  $BA_0 \propto \Phi_0$ , where  $\Phi_0$  is the magnetic flux quantum. However, as has been recently shown for ballistic and diffusive two-dimensional hole gases (based on the  $4 \times 4$  Luttinger Hamiltonian) [34], an underlying Berry phase gives rise to a characteristic shift of the WL peak. This shift depends on the associated Berry phase  $\Gamma$  and the typical accumulated angle  $\alpha_0$ . Moreover, for diffusive and chaotic conductors there is a finite classical correlation  $\rho$  between the random variables  $A$  and  $\alpha$ . These different quantities determine an effective magnetic “Berry field”  $\tilde{B}$  by which the WL magneto profile is shifted. For a chaotic quantum dot, this shift corresponds to an associated flux [34]

$$\tilde{B} A_0 \propto \left( \Gamma \rho \frac{\alpha_0}{2\pi} \right) \Phi_0, \quad (14)$$

which depends linearly on the Berry phase  $\Gamma$ , the typical enclosed angle  $\alpha_0$  and the classical correlation  $\rho$ . This behavior has also been found for ballistic cavities based on HgTe [39]. For the disordered HgTe quantum well, we expect a corresponding behaviour, not only for the WL, but also for the WAL peaks.

Fig. 4(a) shows the numerically obtained quantum correction to the magnetoconductance  $\delta T_U$  (bullets) based on the upper block U of the Hamiltonian (1). The five different curves correspond to different Fermi energies, close to  $E_F = 52$  nm, labeled by the number of open transverse modes (without spin) varying from 30 to 45. Fits to the numerical data are shown as solid lines. Correspondingly, the dashed lines show the further contribution from the lower block L. The curves exhibit a small but distinct energy-dependent shift in  $B$ , respectively, a splitting of the magnetoconductance of different blocks. This feature can be explained in terms of the Berry field introduced above. To this end, the Berry phase  $\Gamma$  corresponding to the Fermi energy  $E$ , respectively, a number of open modes is shown in Fig. 4(b). Since  $\Gamma$  is close to  $\pi$  in the energy range shown, all magnetoconductance curves show WAL. Most notably, the sign change in  $\Gamma - \pi$  between energies corresponding to 36 and 37 channels in Fig. 4(b) is reflected in the direction of the energy dependent shift of the WAL curves in Fig. 4(a), with a nearly vanishing shift close to the trace with  $n = 37$ . Hence, Fig. 4(b) illustrates the transition from negative correction to positive correction between 36 and 37 open channels. The same transition is also visible in the effective Berry field  $\tilde{B}$ , which we extracted for various magnetoconductance curves by the same fits as shown in Fig. 4(a). The effective Berry field  $\tilde{B}$  is depicted in Fig. 4(c). In view of Fig. 4(b) its energy dependence indicates a linear dependence on the Berry phase as it is the case in chaotic quantum dots, see Eq. (14) [34]. Due to the relatively low correlation  $\rho$  between  $\alpha$  and  $A$  for a diffusive process, we expect the strength of the shift to be only a few  $\mu T$  in the present case. However, such a shift leads to a significant change of the magnetoresistance line shape. To the best of our knowledge, it is not captured by any existing diagrammatic approach or description by random matrix theory.

#### IV. ROLE OF SPIN-ORBIT INTERACTION

In addition to the spin-orbit coupling between the  $s$ - and  $p$ -bands within the  $2 \times 2$  blocks, there are further spin-orbit interactions present in HgTe heterostructures. Those can be divided due to their physical origin into terms arising from bulk inversion asymmetry (BIA) and structure inversion asymmetry (SIA). BIA is given by the crystal structure itself, and thus can only be modified by changing the material. SIA depends on internal and external electric fields, and consequently changes its size depending on the symmetries of the grown HgCdTe layers or external gating. For symmetric HgTe quantum wells the strength of SIA is negligibly small.

In the following, we first focus on the WAL profile in a symmetric heterostructure with a naturally sized BIA and without SIA. Our results for different Fermi energies are summarized in Fig. 5(a) for inverted band ordering and in Fig. 5(b) for conventional band ordering.

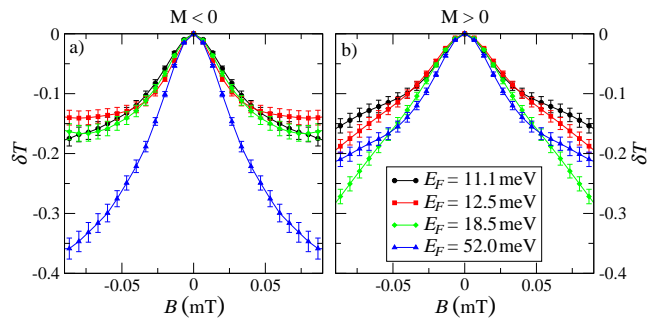


FIG. 5: Strength of the WL correction  $\delta T$  in presence of spin-orbit interaction due to structure inversion asymmetry ( $\Delta = 1.6$  meV) for (a) inverted band order ( $M = -10$  meV) and (b) conventional band order ( $M = +10$  meV).

The energies are chosen to cover the full range of Berry phases as in Fig. 3. In comparison to systems without additional SOI the average magnetoconductance always features WAL. This is in line with the common explanation that strong SOI leads to spin relaxation and thereby WAL. However, there exists a significant difference between the energy dependence of the WAL strength for the different band orderings. For conventional ordering, the WAL correction is almost constant and also the shape of the correction does not change significantly with Fermi energy, as shown in Fig. 5(b). This is not the case for the inverted ordering. Here, the correction is almost twice as strong if the Fermi energy is chosen to be  $E_e^{(\pi)} = 52$  meV, Eq. (12), the point with a Berry phase of  $\pi$ , as depicted in Fig. 5(a).

In the following, we give an explanation for this difference. To this end, we apply the unitary transformation

$$\mathcal{T} = \frac{1}{\sqrt{2}} \begin{pmatrix} 1 & 0 & 0 & 1 \\ 0 & -1 & 1 & 0 \\ -1 & 0 & 0 & 1 \\ 0 & 1 & 1 & 0 \end{pmatrix} \quad (15)$$

to the Hamiltonian (1), leading to the transformed Hamiltonian

$$H = \begin{pmatrix} C_k - \Delta & -Ak_+ & -M_k & -i\frac{1}{2}Rk_- \\ -Ak_- & C_k - \Delta & -\frac{1}{2}iRk_+ & M_k \\ -M_k & \frac{1}{2}iRk_- & C_k + \Delta & -Ak_+ \\ \frac{1}{2}iRk_+ & M_k & -Ak_- & C_k + \Delta \end{pmatrix}. \quad (16)$$

If no SOI due to SIA is present ( $R = 0$ ), this Hamiltonian consists of two blocks which are only coupled by the matrix element  $M_k = M - Bk^2$ . For an inverted band ordering there exists a momentum  $\mathbf{k}$ , where  $M_k \approx 0$  since  $M$  and  $B$  are both negative. In HgTe superstructures with  $M = -10$  meV the Fermi energy is 52 meV corresponding to  $E_e^{(\pi)}$ . At this energy the Hamiltonian decouples into two independent  $2 \times 2$  blocks that both show WAL. Thus the entire WAL strength is twice as high compared to other energies, as shown in Fig. 5(a).

If additional spin-orbit terms from SIA are present, this unitary transformation into two uncoupled blocks

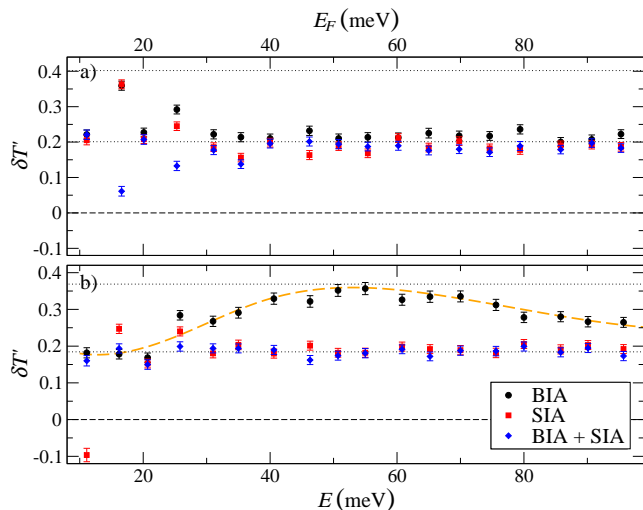


FIG. 6: Strength of the WL correction  $\delta T'$  for different spin-orbit interactions (BIA  $\Delta = 1.6$  meV, SIA  $R = 35$  eV $\text{\AA}$ ). Results are extracted from the transmission at 0.1 mT. a) The localization strength for conventional band ordering ( $M = 10$  meV) shows the same localization strength for all combinations of structure and bulk inversion asymmetry. b) For inverted band ordering ( $M = -10$  meV) and pure structure inversion asymmetry, the strength of the WAL correction is doubled at  $E_c^{(\pi)} = 52$  meV.

is not possible. As a consequence, the WAL correction stays roughly constant throughout the whole range of different Fermi energies. In Fig. 6 we have summarized the behaviour of the WAL correction  $\delta T'$ , Eq. (13), for different combinations of BIA and SIA. As expected, the WAL with conventional band ordering is independent of the type of SOI, as shown in Fig. 6(a). However, this is not the case for a heterostructure with inverted band ordering. If only BIA is present, WAL is approximately doubled at 52 meV and shows a smooth transition in between, see black symbols in Fig. 6(b). For finite SIA a block diagonalization is not possible, and hence the WAL correction is constant, independent of whether additional

BIA SOI is present. As in the calculations without SOI, the erratic fluctuations of the WAL strength at low energies can be attributed to the correspondingly limited amount of open channels in the numerical calculations.

## V. CONCLUSION

In this manuscript, we have analyzed the weak localization properties of HgTe heterostructures with different band topologies. We revealed a transition between weak localization and weak antilocalization for systems without spin-orbit interaction, which is only complete for systems with inverted band ordering and can be related to the effect of the Berry phase. This Berry phase, moreover, affects the magnetoconductance line shape: Owing to correlations in the statistics of backscattered paths that depends on the type of classical dynamics (diffusive, chaotic or regular in the ballistic case) the Berry phase implies a splitting of the magnetoconductance profile. Furthermore, we showed that the band ordering can be deduced from the energy dependence of the weak antilocalization correction in presence of spin-orbit interaction due to bulk inversion asymmetry: If the heterostructure features an inverted band ordering, the correction strength is energy dependent in contrast to a constant weak antilocalization strength for conventional band ordering. This is explained by an energy-dependent separation into two uncoupled blocks. Additional Rashba-type spin-orbit interaction from structure inversion asymmetry again diminishes the energy dependence.

## Acknowledgments

This work is supported by Deutsche Forschungsgemeinschaft (GRK 1570 and joined DFG-JST Forschergruppe Topological Electronics). We thank I. Adagideli, E. Hankiewicz, G. Tkachov and M. Wimmer for useful conversations.

- 
- [1] C. L. Kane and E. J. Mele, *Quantum Spin Hall Effect in Graphene*, *Phys. Rev. Lett.* **95**, 226801 (2005).
  - [2] C. L. Kane and E. J. Mele, *Z Topological Order and the Quantum Spin Hall Effect*, *Phys. Rev. Lett.* **95**, 146802 (2005).
  - [3] D. Huertas-Hernando, F. Guinea and A. Brataas, *Spin-orbit coupling in curved graphene, fullerenes, nanotubes, and nanotube caps*, *Phys. Rev. B* **74**, (2006).
  - [4] M. Gmitra, S. Konschuh, C. Ertler, C. Ambrosch-Draxl and J. Fabian, *Band-structure topologies of graphene: Spin-orbit coupling effects from first principles*, *Phys. Rev. B* **80**, 235431 (2009).
  - [5] B. A. BERNEVIG, T. L. HUGHES and S.-C. ZHANG, *Quantum Spin Hall Effect and Topological Phase Transition in HgTe Quantum Wells*, *Science* **314**, 1757 (2006).
  - [6] S. Murakami, *Quantum Spin Hall Effect and Enhanced Magnetic Response by Spin-Orbit Coupling*, *Phys. Rev. Lett.* **97**, 236805 (2006).
  - [7] C. Liu, T. Hughes, X.-L. Qi, K. Wang and S.-C. Zhang, *Quantum Spin Hall Effect in Inverted Type-II Semiconductors*, *Phys. Rev. Lett.* **100**, 236601 (2008).
  - [8] L. Fu, C. L. Kane and E. J. Mele, *Topological Insulators in Three Dimensions*, *Phys. Rev. Lett.* **98**, 106803 (2007).
  - [9] L. Fu and C. L. Kane, *Topological insulators with inversion symmetry*, *Phys. Rev. B* **76**, 45302 (2007).
  - [10] D.-X. Qu, Y. S. Hor, J. Xiong, R. J. Cava and N. P. Ong, *Quantum Oscillations and Hall Anomaly of Surface States in the Topological Insulator BiTe*, *Science* **329**, 821 (2010).

- [11] F. Xiu *et al.*, *Manipulating surface states in topological insulator nanoribbons*, *Nat. Nano* **6**, 216 (2011).
- [12] M. König, S. Wiedmann, C. Brüne, A. Roth, H. Buhmann, L. W. Molenkamp, X.-L. Qi and S.-C. Zhang, *Quantum Spin Hall Insulator State in HgTe Quantum Wells*, *Science* **318**, 766 (2007).
- [13] A. Roth, C. Brüne, H. Buhmann, L. W. Molenkamp, J. Maciejko, X.-L. Qi and S.-C. Zhang, *Nonlocal Transport in the Quantum Spin Hall State*, *Science* **325**, 294 (2009).
- [14] I. Knez, R.-R. Du and G. Sullivan, *Evidence for Helical Edge Modes in Inverted InAs/GaSb Quantum Wells*, *Phys. Rev. Lett.* **107**, 136603 (2011).
- [15] B. Zhou, H.-Z. Lu, R.-L. Chu, S.-Q. Shen and Q. Niu, *Finite Size Effects on Helical Edge States in a Quantum Spin-Hall System*, *Phys. Rev. Lett.* **101**, 246807 (2008).
- [16] L. B. Zhang, F. Cheng, F. Zhai and K. Chang, *Electrical switching of the edge channel transport in HgTe quantum wells with an inverted band structure*, *Phys. Rev. B* **83**, 81402 (2011).
- [17] V. Krueckl and K. Richter, *Switching Spin and Charge between Edge States in Topological Insulator Constrictions*, *Phys. Rev. Lett.* **107**, 86803 (2011).
- [18] F. Dolcini, *Full electrical control of charge and spin conductance through interferometry of edge states in topological insulators*, *Phys. Rev. B* **83**, 165304 (2011).
- [19] J. C. Budich, F. Dolcini, P. Recher and B. Trauzettel, *Phonon-Induced Backscattering in Helical Edge States*, *Phys. Rev. Lett.* **108**, 086602 (2012).
- [20] B. Altshuler, D. Khmel'nitzkii, A. Larkin and P. Lee, *Magnetoresistance and Hall effect in a disordered two-dimensional electron gas*, *Phys. Rev. B* **22**, 5142 (1980).
- [21] S. Hikami, A. I. Larkin and Y. Nagaoka, *Spin-Orbit Interaction and Magnetoresistance in the Two-Dimensional Random System*, *Prog. Theor. Phys.* **63**, 707 (1980).
- [22] H.-T. He, G. Wang, T. Zhang, I.-K. Sou, G. Wong, J.-N. Wang, H.-Z. Lu, S.-Q. Shen and F.-C. Zhang, *Impurity Effect on Weak Antilocalization in the Topological Insulator  $Bi_{2-x}Te_3$* , *Phys. Rev. Lett.* **106**, 166805 (2011).
- [23] G. Tkachov and E. M. Hankiewicz, *Weak antilocalization in HgTe quantum wells and topological surface states: Massive versus massless Dirac fermions*, *Phys. Rev. B* **84**, 035444 (2011).
- [24] E. B. Olshanetsky, Z. D. Kvon, G. M. Gusev, N. N. Mikhailov, S. A. Dvoretzky and J. C. Portal, *Weak antilocalization in HgTe quantum wells near a topological transition*, *JETP Letters* **91**, 347 (2010).
- [25] G. M. Minkov, A. V. Germanenko, O. E. Rut, A. A. Sherstobitov, S. A. Dvoretzki and N. N. Mikhailov, *Weak antilocalization in HgTe quantum well with inverted energy spectrum*, arXiv:1202.1093 (2012).
- [26] S. V. Iordanskii, Y. B. Lyanda-Geller and G. E. Pikus, *Weak localization in quantum wells with spin-orbit interaction*, *JETP Lett.* **60**, 206 (1994).
- [27] W. Knap *et al.*, *Weak antilocalization and spin precession in quantum wells*, *Phys. Rev. B* **53**, 3912 (1996).
- [28] D. G. Rothe, R. W. Reinthaler, C.-X. Liu, L. W. Molenkamp, S.-C. Zhang and E. M. Hankiewicz, *Fingerprint of different spin-orbit terms for spin transport in HgTe quantum wells*, *New J. Phys.* **12**, 65012 (2010).
- [29] M. König, H. Buhmann, L. W. Molenkamp, T. L. Hughes, C.-X. Liu, X.-L. Qi and S.-C. Zhang, *The Quantum Spin Hall Effect: Theory and Experiment*, *J. Phys. Soc. Jpn.* **77**, 31007 (2008).
- [30] R. Landauer, *Electrical resistance of disordered one-dimensional lattices*, *Philosophical Magazine* **21**, 863 (1970).
- [31] D. S. Fisher and P. A. Lee, *Relation between conductivity and transmission matrix*, *Phys. Rev. B* **23**, 6851 (1981).
- [32] M. V. Berry, *Quantal phase factors accompanying adiabatic changes*, *Proc. R. Soc. Lond. A* **392**, 45 (1984).
- [33] M.-C. Chang and Q. Niu, *Berry phase, hyperorbits, and the Hofstadter spectrum: Semiclassical dynamics in magnetic Bloch bands*, *Phys. Rev. B* **53**, 7010 (1996).
- [34] V. Krueckl, M. Wimmer, I. Adagideli, J. Kuipers and K. Richter, *Weak Localization in Mesoscopic Hole Transport: Berry Phases and Classical Correlations*, *Phys. Rev. Lett.* **106**, 146801 (2011).
- [35] H. Suzuura and T. Ando, *Crossover from Symplectic to Orthogonal Class in a Two-Dimensional Honeycomb Lattice*, *Phys. Rev. Lett.* **89**, 266603 (2002).
- [36] E. McCann, K. Kechedzhi, V. I. Falko, H. Suzuura, T. Ando and B. L. Altshuler, *Weak-Localization Magnetoresistance and Valley Symmetry in Graphene*, *Phys. Rev. Lett.* **97**, 146805 (2006).
- [37] M. V. Berry and R. J. Mondragon, *Neutrino billiards: time-reversal symmetry-breaking without magnetic fields*, *Proc. R. Soc. Lond. A* **412**, 53 (1987).
- [38] C. W. J. Beenakker, *Random-matrix theory of quantum transport*, *Rev. Mod. Phys.* **69**, 731 (1997).
- [39] See supplementary material of Ref. [34].